Journal of Biomedical Optics

SPIEDigitalLibrary.org/jbo

Lens-free computational imaging of capillary morphogenesis within three-dimensional substrates

John Weidling
Serhan O. Isikman
Alon Greenbaum
Aydogan Ozcan
Elliot Botvinick

SPIE

Lens-free computational imaging of capillary morphogenesis within three-dimensional substrates

John Weidling,[a] Serhan O. Isikman,[b] Alon Greenbaum,[b] Aydogan Ozcan,[b,c,d] and Elliot Botvinick[a,e,f]
[a]University of California Irvine, Biomedical Engineering Department, Irvine, California
[b]University of California Los Angeles, Electrical Engineering Department, Los Angeles, California
[c]University of California Los Angeles, Bioengineering Department, Los Angeles, California
[d]University of California Los Angeles, California NanoSystems Institute, Los Angeles, California
[e]University of California Irvine, Beckman Laser Institute, Irvine, California
[f]University of California Irvine, Edwards Lifesciences Center for Advanced Cardiovascular Technology, Irvine, California

Abstract. Endothelial cells cultured in three-dimensional (3-D) extracellular matrices spontaneously form microvessels in response to soluble and matrix-bound factors. Such cultures are common for the study of angiogenesis and may find widespread use in drug discovery. Vascular networks are imaged over weeks to measure the distribution of vessel morphogenic parameters. Measurements require micron-scale spatial resolution, which for light microscopy comes at the cost of limited field-of-view (FOV) and shallow depth-of-focus (DOF). Small FOVs and DOFs necessitate lateral and axial mechanical scanning, thus limiting imaging throughput. We present a lens-free holographic on-chip microscopy technique to rapidly image microvessels within a Petri dish over a large volume without any mechanical scanning. This on-chip method uses partially coherent illumination and a CMOS sensor to record in-line holographic images of the sample. For digital reconstruction of the measured holograms, we implement a multiheight phase recovery method to obtain phase images of capillary morphogenesis over a large FOV (24 mm^2) with ~1.5 μm spatial resolution. On average, measured capillary length in our method was within approximately 2% of lengths measured using a 10× microscope objective. These results suggest lens-free on-chip imaging is a useful toolset for high-throughput monitoring and quantitative analysis of microvascular 3-D networks.
 [DOI: 10.1117/1.JBO.17.12.126018]

Keywords: three-dimensional culture; capillary morphogenesis; tissue engineering; angiogenesis; lens-free imaging; on-chip microscopy; computational microscopy; holographic microscopy.

Paper 12536 received Aug. 19, 2012; revised manuscript received Nov. 14, 2012; accepted for publication Nov. 19, 2012; published online Dec. 13, 2012.

1 Introduction

Conventional light microscopy has been a vital tool in the life sciences by giving noninvasive visual access to micro-objects such as cells and microorganisms. Although significant improvements have been achieved to improve spatial resolution and contrast,[1–12] one important restriction of light microscopy for many applications has been the limited field-of-view (FOV) and depth-of-focus (DOF). That is, for applications where large areas and/or volumes need to be screened, one typically needs to mechanically scan the sample under the microscope, demanding long scan times and relatively complex hardware. Lens-free on-chip holographic microscopy offers an alternative platform that overcomes this limitation.[13–25] Unlike conventional light microscopy, lens-free on-chip microscopy does not rely on optical magnification. Instead, it uses the emerging large-format sensor architectures with small pixel sizes together with novel imaging algorithms to compensate for the lack of optical components such as lenses or objectives. Therefore, it enables imaging large areas (e.g., >24 to 30 mm^2) at submicrometer spatial resolution in a compact and cost-effective set-up.[18,19,21–25]

In addition to the limited FOV, the short DOF associated with objective lenses poses further challenges, especially if the sample has a three-dimensional (3-D) structure, such as a tissue culture in a Petri dish where objects might be distributed at different depths. For such 3-D samples, in addition to lateral scanning, re-focusing by depth-scanning also becomes necessary. While high-end microscopes can perform both lateral and depth scanning automatically, these systems are cost-prohibitive and bulky. In contrast, lens-free on-chip holographic imaging provides particular advantages by offering the ability to perform postexposure digital auto-focusing (or depth-scanning) using holographic reconstruction over a depth-of-field of up to ~4 to 5 mm.[21,22] Owing to the partially coherent holographic image acquisition scheme (unlike e.g., contact imaging techniques) the detector records the information regarding the entire 3-D structure of the sample, and lens-free images can be digitally reconstructed at any depth of interest over an extended depth-of-field.[21,22]

One important biological system that can be observed at the scale and resolution of lens-free imaging is a cultured microvascular capillary network. The study of capillary network formation, or capillary morphogenesis and angiogenesis, is vital to the fields of wound healing and tissue engineering of prevascularized implants,[26] tumor mediated vascularization,[27] and various diseases.[28] Often times the growth and morphology of a complex capillary network must be monitored and quantified over many days in order to determine the effects of experimental conditions such as the addition of a putative drug.[29] Capillary tubule

Address all correspondence to: Elliot Botvinick, University of California, Irvine, California. Tel: 949-824-9613; Fax: 949-824-9968; E-mail: elliot.botvinick@uci.edu

0091-3286/2012/$25.00 © 2012 SPIE

formation is commonly quantified by the average tubule length, number of tubules, tubule area, and number of branch points.[30] Since such measurements require micron-scale resolution, samples are traditionally imaged by conventional light microscopy, which due to its small FOV and shallow DOF precludes rapid quantification of the entire culture volume. As a compromise, results are averaged across a discrete number of regions using a time-intensive process.[31–37] Numerous image analysis algorithms including packages for NIH ImageJ, Analyze Skeleton and AngioQuant[38,39] have been developed for accurate hands-free quantification of capillary growth,[31,33,40] leaving image acquisition as the primary rate-limiting step. While commercial high content imaging systems (e.g., BD Pathway 855) can scan the entire sample in 3-D, these systems are relatively expensive and slow because they rely on mechanical scanning.

In contrast to existing approaches, our lens-free on-chip technique enables imaging of the entire sample with sufficient resolution to draw statistical conclusions regarding changing morphology using existing image processing techniques. To demonstrate its proof of concept, here we present the use of lens-free on-chip microscopy to image capillaries grown in a 3-D *in vitro* system, without the use of lenses or mechanical scanning, and with sufficient spatial resolution to accurately determine vessel number, vessel length and vessel area.

2 Materials and Methods

2.1 *Capillary Morphogenesis Model*

A model for capillary morphogenesis as first described by Nehls and Drenckhahn was implemented in Ref. 41. Primary human umbilical vein endothelial cells (HUVECs) were grown on microcarrier beads imbedded in a crosslinked fibrin hydrogel and given pro-angiogenic signaling factors naturally released by fibroblast cells cultured on top of the gel. HUVECs were first expanded in cell culture flasks to passage number three and then cultured on the surface of 150 to 210 μm diameter carrier beads (Cytodex). Beads were immersed in a 2.5 mg/ml solution of fibrinogen (bovine, Sigma) in EBM-2 media (Lonza) at approximately 100 beads/ml solution. The solution was then pipetted into a 35 mm diameter Petri dish with type 1 glass bottom (MatTek) containing 20 μl of thrombin (Sigma). A clotting cascade forms a fibrin gel thus imbedding the carrier beads within a 3-D extracellular matrix. Once the gel is formed, normal human lung fibroblast cells (NHLFs) grown out to passage five were seeded onto a Transwell container (Corning) that is placed on top of the gel allowing signaling factors released by the fibroblasts to diffuse down into the gel while keeping the fibroblasts mechanically separated from the gel (Fig. 1). Next, 2 ml of EGM-2 media (Lonza) was added to each sample with media exchanged every other day. Capillary sprouting from the carrier beads begins by day two with large interconnected capillary networks forming by day seven. Imaging was performed on day seven.

2.2 *Lens-free On-Chip Imaging Setup*

The lens-free on-chip imaging setup, shown in Fig. 1, is composed of a partially coherent light source and an opto-electronic sensor array (complementary metal-oxide-semiconductor (CMOS) Model #MT9P031, Micron Technology; pixel size: 2.2 μm, 5 mega pixels). The sample is placed directly on the top of the sensor chip such that the distance, z_2, between the objects and the active area of the detector is ~1 to 2 mm. The sample is illuminated using a near infrared light emitting diode (LED, $\lambda = 950$ nm) that is butt-coupled to a multimode optical fiber that has a core-diameter of 100 μm. The distance, z_1, between the light source and the sample is typically ~10 cm, and its placement does not require sensitive alignment.

An infrared LED was selected in our imaging experiments since it was found to reduce the background noise from multiple

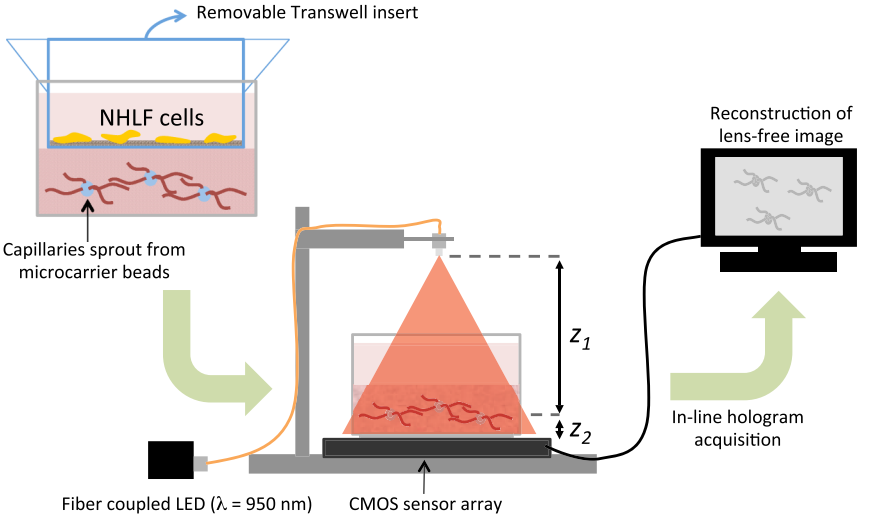

Fig. 1 Schematic of our tissue culture system and lens-free computational imaging apparatus. NHLF fibroblasts are cultured on the top surface of a Transwell insert, which is placed within a 35 mm glass-bottom Petri dish. HUVECs were first cultured onto microcarrier beads, which were then embedded within a crosslinked fibrin hydrogel. Soluble signals released from the fibroblasts stimulate the HUVECs to spontaneously form capillaries. The insert was removed prior to imaging. A partially coherent fiber-coupled LED light source illuminates the Petri dish, which is placed above the CMOS chip to record the holographic image of the sample over a large field-of-view and extended depth-of-field; z_1 is the distance between the light source and the object; z_2 is the distance between the objects (capillaries) and the active area of the detector, which is changed by placing or removing a glass coverslip underneath the sample. A computer reconstructs lens-free images according to described algorithms.

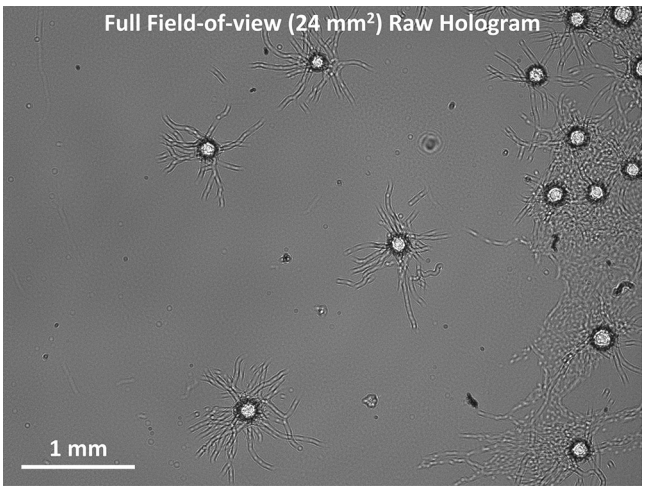

Fig. 2 A full FOV hologram of a sample placed on the sensor array. The unit magnification holographic recording scheme permits imaging and monitoring capillaries over a large FOV of 24 mm^2, that equals the active area of the CMOS detector array.

scattering within the fibrin gel, and this also minimizes the phase-wrapping problems in the reconstructed lens-free phase images as phase delay is inversely proportional to the wavelength. Since the light impinging on the sample is partially coherent both temporally and spatially,[13,14] the unperturbed portion of the illumination interferes with the waves scattered by the objects. The sensor records this interference pattern, i.e., an in-line hologram of the objects placed on the chip. Owing to its unique geometrical configuration where $z_1 \gg z_2$, in-line holograms are recorded with unit magnification over a large imaging FOV that equals the active area of the sensor-array, in this case 24 mm^2 (Fig. 2), which can further increase to e.g., >15 cm^2 with a different choice of sensor-array.[16]

2.3 *Digital Holographic Reconstruction*

Lens-free images are reconstructed using digital beam propagation techniques based on the angular spectrum approach.[42] In this approach, lens-free images are convolved with the impulse response of free space propagation. This operation is done in the Fourier domain, by multiplying the 2D Fourier transform of lens-free images with the transfer function of free space propagation, which can be expressed as:[42]

$$H_c(f_x,f_y)=\begin{cases} e^{j2\pi z\left[1-(\lambda f_x)^2-(\lambda f_y)^2\right]^{1/2}} & \sqrt{f_x^2+f_y^2}\le\frac{1}{\lambda} \\ 0 & \text{otherwise} \end{cases}. \quad (1)$$

In Eq. (1), f_x and f_y denote spatial frequencies of the input field along x and y, respectively, λ is the illumination wavelength in free space, and z is the distance to which the original field is propagated. After multiplication by this transfer function, an inverse Fourier transform provides the output at the desired plane.

When the above-mentioned digital beam-propagation is performed on the measured lens-free holograms, the reconstructed images exhibit artifacts due to the "twin-image" noise. Stated differently, since imaging sensors are only sensitive to the intensity of an optical field, the initial phase of the complex field at the hologram plane, which is unknown, is assumed to be zero before digital propagation, giving rise to artifacts in the reconstructed image. In order to obtain a refined reconstructed image that does not suffer from this twin-image noise, phase recovery algorithms should be used to retrieve the unknown phase at the hologram plane. One way of achieving this is to use a size-constrained iterative phase recovery algorithm,[14] where the object size is used as additional information (i.e., size-constraint) in the reconstruction process. The object size can generally be estimated from the initial reconstruction despite the contamination due to the twin-image noise, as the boundaries of the objects can still be determined. For lens-free imaging of capillaries, however, the complex morphology of the sample makes it challenging to estimate the capillary shape and size, hampering the use of size-constrained phase recovery algorithms. As a result, here we utilized an alternative phase-recovery algorithm, multi-height phase recovery (MHPR),[24,25,43] which does "not" require the knowledge of the object size or shape as additional information, but instead uses multiple intensity measurements.

2.4 *Multi-Height Phase Recovery*

In this iterative phase-retrieval technique, multiple in-line holograms (i.e., intensity measurements) are recorded for the same object, where each measurement is performed at a different z_2 distance. For lens-free imaging of capillaries, two intensity measurements were sufficient to effectively retrieve the phase of the optical field at the hologram plane. The change in z_2 distance is achieved by placing or replacing a coverslip with a thickness of, for example, ~150 μm as a spacer between the sample and the sensor. This operation may also cause a slight translation and rotation of the sample with respect to the sensor array between two successive lens-free image acquisitions. Therefore, the two measured lens-free holograms are first registered to each other in order to compensate for any translational or rotational motion. The exact z_2 distances do not need to be known a priori, since an auto-focus algorithm[17] as described below is utilized to estimate this parameter. After image registration, the MHPR algorithm is invoked to retrieve the missing phase of the sample holograms. The algorithm works by propagating the measured fields back and forth between the two planes of measurement. At each iteration, the algorithm enforces the recorded (i.e., measured) amplitude at the corresponding height (i.e., z_2), while keeping the updated phase for the next iteration. This way, the missing phase is retrieved in ~10 iterations without modifying the measured amplitude values, resulting in a refined lens-free image where the twin-image noise is significantly suppressed.

2.5 *Digital Autofocusing Algorithm*

An important attribute of lens-free holography is that it enables imaging of samples over a long depth-of-field, as long as the holograms of objects at large distances above the sensor (e.g., 1 to 5 mm) have sufficient signal-to-noise ratio.[21,22] This ability is particularly useful for imaging capillary morphogenesis due to the inherent 3-D nature of the sample. Imaging an extended depth-of-field is achieved by reconstructing the holograms at different depths-of-interest, which is equivalent to focusing a conventional microscope objective lens at different depths. However, digitally selecting the object-to-detector distance (z_2), which maximizes the contrast and the signal-to-noise ratio of the object, can be a tedious task when imaging objects over a large volume. Towards this end, we implemented an autofocus algorithm to automatically determine the best

plane of focus for imaging different capillaries across the sample volume.[17]

This autofocus algorithm is based on the fact that the edges of the object should be the sharpest at the plane of best focus. To estimate the sharpness of the edges, first a Sobel operator is used to detect edges in the vertical and horizontal directions. Second, the edge images are combined by using the two-norm (i.e., the square root of the sum of the squares). Third, the variance of the resultant image is calculated, where a high variance indicates existence of sharp edges. Therefore our autofocus algorithm scans several z_2 distances spaced by e.g., 1 μm distances in order to find the z_2 distance with the maximum edge variance, i.e., the best focus. It should be noted that this auto-focus algorithm is invoked twice in order to estimate the z_2 distances for both measurement planes. For a typical sample, the difference in the z_2 distances of the two lens-free holograms does not exceed 50 μm. Consequently, once the z_2 distance for one of the lens-free holograms is determined, the search space for the z_2 distance of the second hologram is rather small, achieving fast convergence.

3 Results and Discussion

To obtain microscopic 3-D images of the sample, the recorded lens-free in-line holograms are digitally reconstructed[14] where the recorded amplitude is initially multiplied by a reference plane wave and the resulting optical field is back-propagated[42] to the sample/object plane. Due to the in-line holographic recording scheme, the reconstructed images exhibit twin image noise [e.g., Fig. 3(a2) and 3(b2)], which degrades the lens-free image quality by concealing an object's fine features and giving rise to artificial intensity modulations that may lead to a biological misinterpretation. The arrows in Fig. 3 point to exemplary regions where the twin image hampers accurate interpretation of the reconstructed images, either by concealing the actual structure, or sometimes creating artifacts that misleadingly appear like capillaries.

To digitally eliminate this twin image noise, as detailed in Sec. 2, a MHPR algorithm is invoked to enable accurate interpretation of our lens-free reconstructed images. A visual comparison of Fig. 3(a3) and 3(b3) to 3(a2) and 3(b2), particularly in the regions indicated by the arrows, clearly demonstrates the significance of our MHPR approach to lens-free 3-D imaging of capillaries. Figure 3(a4) and 3(b4) further demonstrate this improvement by showing profiles along the white lines in 3(a2), 3(b2), 3(a3), and 3(b3). These plots illustrate that using multi-height phase retrieval the modulations due to capillaries get stronger, increasing the image contrast, while false modulations due to the twin-image artifacts are now significantly suppressed.

It should be noted that pixel super-resolution techniques that digitally increase the spatial resolution of lens-free on-chip imaging were not implemented here.[18,19,21–23] As a result, the lens-free imaging platform utilized here provides a modest spatial resolution of ~1.5 to 2.0 μm (still subpixel considering that the CMOS chip has a pixel size of 2.2 μm),[14] which was more than sufficient for the quantitative analysis of vessel length in our application. We compared the average capillary length of a 3-D sample measured by both the MHPR-based lens-free microscopy [Fig. 4(a)] and an inverted microscope with a 10× objective lens (Nikon, NA = 0.1) under bright field illumination [Fig. 4(b)]. In these measurements, capillary length was estimated as the linear distance from the center of the bead to the tip of each capillary. Based on these measurements, vessel length differences between the two methods were found to

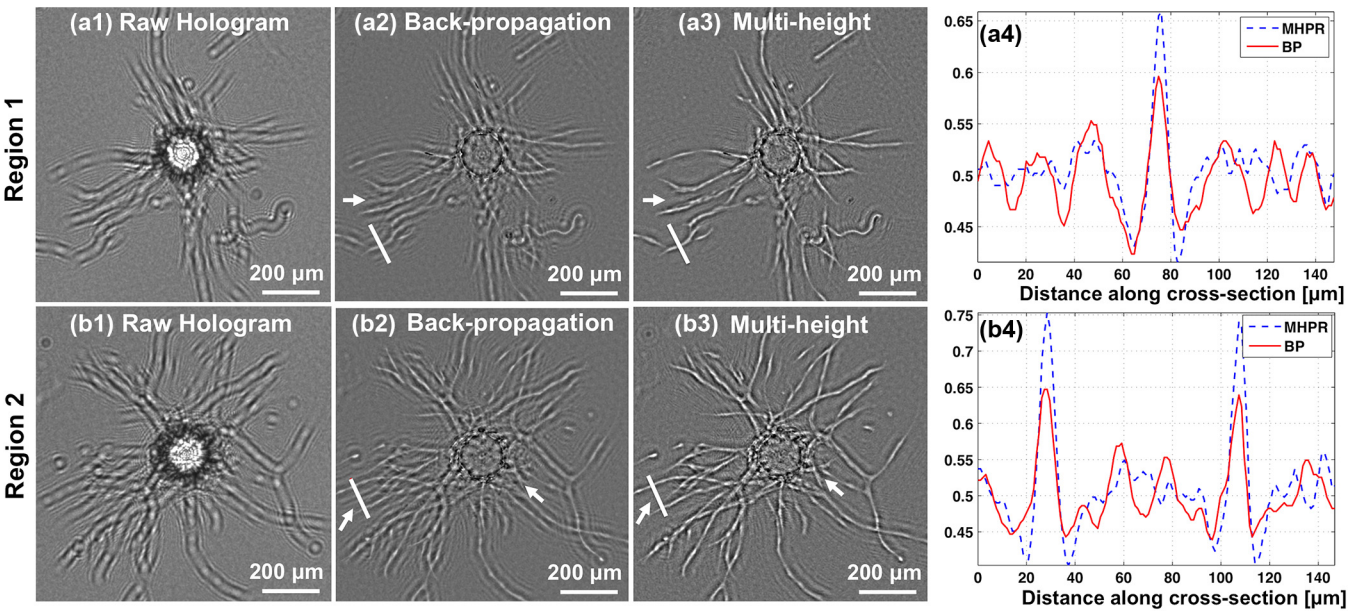

Fig. 3 (a1, b1) Cropped raw holograms for region 1 and region 2 of Fig 2. (a2, b2) Reconstructed lens-free images after back-propagation (BP) without MHPR. (a3, b3) Reconstructed images using MHPR. This approach retrieves the phase of the hologram, and therefore effectively removes the twin image noise from the reconstructed images shown in (a2, b2). The arrows point to exemplary regions where removal of the twin-image noise is of particular importance, as it otherwise gives rise to artifacts that could be misinterpreted as capillaries. (a4, b4) Line profiles along the white lines in (a2, a3) and (b2, b3), respectively. These plots reveal that while the modulations due to capillaries get stronger in the line profiles with MHPR, false modulations due to the twin-image artifacts are significantly suppressed, further demonstrating the refinement and contrast enhancement in the lens-free images obtained by MHPR.

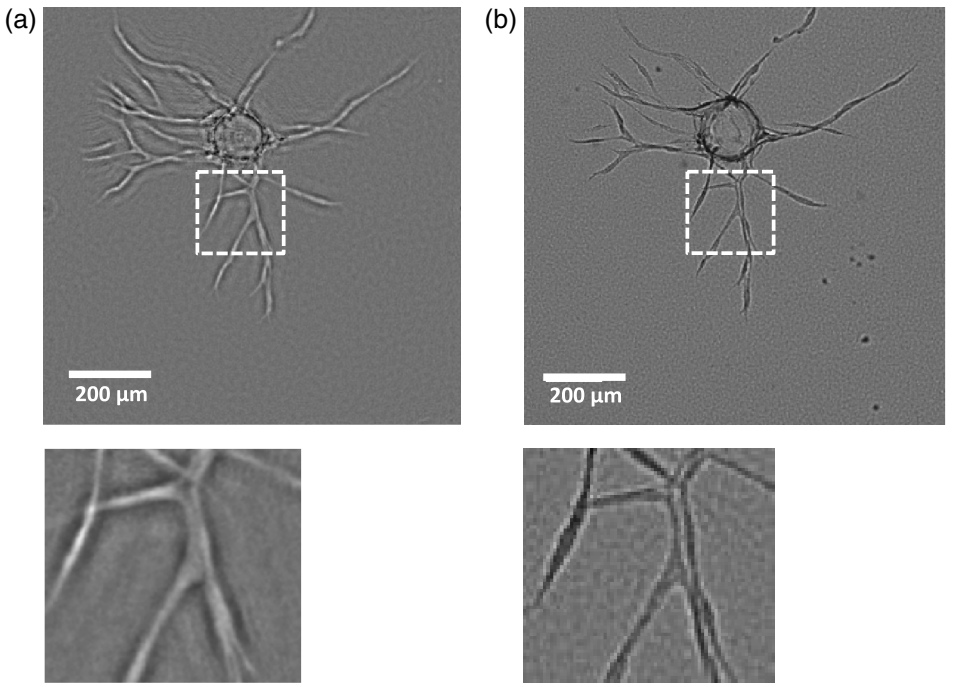

Fig. 4 (a) Reconstructed image of a carrier bead and capillaries using MHPR. The zoomed region clearly shows sufficient resolution and contrast to delineate bifurcations highlighting micron-scale resolution. (b) The same carrier bead imaged with an inverted microscope and a 10× objective lens under bright field illumination. While the relative contrasts are reversed, key morphological features can be extracted from either the MHPR or the conventional microscope image.

be less than 2% indicating that lens-free imaging can faithfully replace traditional microscopy in our model system. Importantly, the lens-free system has the advantage of its extraordinarily large FOV and DOF. The microscopic image shown in Fig. 4(b) acquired with a 10× objective lens has a FOV of 0.86×0.65 mm allowing only one carrier bead to be imaged at a time, while the full FOV of the lens-free image (see Fig. 5) is 24 mm^2 (i.e., >35 fold larger than the FOV of the microscope objective) allowing all the carrier beads to be imaged simultaneously without the need for mechanical scanning. Note that this FOV of the lens-free imaging technique is only limited by the active area of the detector chip, and sample areas larger than e.g., 15 cm^2 can also be imaged by using wide-field CCD sensor-arrays.[16,44]

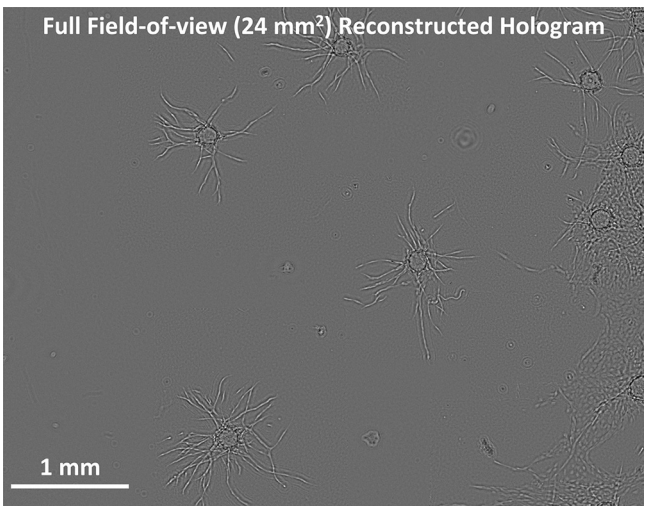

Fig. 5 A full FOV lens-free image of the entire sample after applying the MHPR reconstruction algorithm to the raw hologram of Fig. 2.

In summary, we have demonstrated that imaging of capillary morphogenesis is possible without the use of any lenses or mechanical scanning over a large FOV in 3-D culture. The resolution, image contrast and signal-to-noise-ratio achieved in the reconstructed holographic images were sufficient to extract useful structural information such as vessel length, diameter, area, number of vessels, vessel shape, vessel interactions and the volume fraction of tissue that had been vascularized. The large FOV, depth-of-field, cost-effectiveness, and ease-of-use of the lens-free on-chip imaging platform make it attractive to researchers studying capillary growth under the influence of, for example, chemical or mechanical cues. A high throughput system for measuring growth over large volumes in multiple samples may be possible with the use of lens-free imaging, thus enabling high content screening of 3-D tissue cultures.

Acknowledgments

We wish to acknowledge Dr. Ekaterina Kniazeva for assisting with the capillary culture, Dr. Samir Shreim for assisting with the optical setup and Prof. Christopher Hughes for the supply of HUVECs. E. Botvinick acknowledges the Laser Microbeam and Medical Program (LAMMP), an NIH/NIBIB Biomedical Technology Center (P41EB05890) and the NSF Physical and Engineering Sciences in Engineering program (CMMI-1233697). A. Ozcan also acknowledges the support of the Presidential Early Career Award for Scientists and Engineers (PECASE), ARO Young Investigator Award, NSF CAREER Award, the ONR Young Investigator Award 2009 and the NIH Director's New Innovator Award DP2OD006427 from the Office of The Director, NIH.

References

1. S. A. Jones et al., "Fast, three-dimensional super-resolution imaging of live cells," *Nat. Methods* **8**(6), 499–508 (2011).
2. S. W. Hell, "Toward fluorescence nanoscopy," *Nat. Biotechnol.* **21**(11), 1347–1355 (2003).
3. M. G. L. Gustafsson, "Nonlinear structured-illumination microscopy: wide-field fluorescence imaging with theoretically unlimited resolution," *Proc. Natl. Acad. Sci. U. S. A.* **102**(37), 13081–13086 (2005).
4. E. Betzig et al., "Imaging intracellular fluorescent proteins at nanometer resolution," *Science* **313**(5793), 1642–1645 (2006).
5. M. J. Rust, M. Bates, and X. Zhuang, "Sub-diffraction-limit imaging by stochastic optical reconstruction microscopy (STORM)," *Nat. Methods* **3**(10), 793–796 (2006).
6. S. T. Hess, T. P. Girirajan, and M. D. Mason, "Ultra-high resolution imaging by fluorescence photoactivation localization microscopy," *Biophys. J.* **91**(11), 4258–4272 (2006).
7. Z. Ma et al., "Fluorescence near-field microscopy of DNA at sub-10 nm resolution," *Phys. Rev. Lett.* **97**(26), 260801 (2006).
8. E. Chung et al., "Two-dimensional standing wave total internal reflection fluorescence microscopy: superresolution imaging of single molecular and biological specimens," *Biophys. J.* **93**(5), 1747–1757 (2007).
9. W. R. Zipfel, R. M. Williams, and W. W. Webb, "Nonlinear magic: multiphoton microscopy in the biosciences," *Nat. Biotechnol.* **21**(11), 1369–1377 (2003).
10. W. Choi et al., "Tomographic phase microscopy," *Nat. Methods* **4**(9), 717–719 (2007).
11. R. P. J. Barretto, B. Messerschmidt, and M. J. Schnitzer, "*In vivo* fluorescence imaging with high-resolution microlenses," *Nat. Methods* **6**(7), 511–512 (2009).
12. J. Rosen and G. Brooker, "Non-scanning motionless fluorescence three-dimensional holographic microscopy," *Nat. Photon.* **2**(3), 190–195 (2008).
13. C. Oh et al., "On-chip differential interference contrast microscopy using lensless digital holography," *Opt. Express* **18**(5), 4717–4726 (2010).
14. O. Mudanyali et al., "Compact, light-weight and cost-effective microscope based on lensless incoherent holography for telemedicine applications," *Lab Chip* **10**(11), 1417–1428 (2010).
15. D. Tseng et al., "Lensfree microscopy on a cell-phone," *Lab Chip* **10**(14), 1787–1792 (2010).
16. S. Seo et al., "High-throughput lensfree blood analysis on a chip," *Anal. Chem.* **82**(11), 4621–4627 (2010).
17. O. Mudanyali et al., "Detection of waterborne parasites using field-portable and cost-effective lensfree microscopy," *Lab Chip* **10**(18), 2419–2423 (2010).
18. W. Bishara et al., "Lensfree on-chip microscopy over a wide field-of-view using pixel super-resolution," *Opt. Express* **18**(11), 11181–11191 (2010).
19. W. Bishara et al., "Holographic pixel super-resolution in portable lensless on-chip microscopy using a fiber-optic array," *Lab Chip* **11**(7), 1276–1279 (2011).
20. T. Su et al., "A compact and light-weight automated semen analysis platform using lensfree on-chip microscopy," *Anal. Chem.* **82**(19), 8307–8312 (2010).
21. S. O. Isikman et al., "Field-portable lensfree tomographic microscope," *Lab Chip* **11**(13), 2222–2230 (2011).
22. S. O. Isikman et al., "Lensfree optical tomographic microscope with a large imaging volume on a chip," *Proc. Nat. Acad. Sci. U. S. A.* **108**(18), 7296–7301 (2011).
23. S. O. Isikman et al., "Optofluidic tomography on a chip," *Appl. Phys. Lett.* **98**(16), 161109 (2011).
24. A. Greenbaum and A. Ozcan, "Maskless imaging of dense samples using pixel super-resolution based multi-height lensfree on-chip microscopy," *Opt. Express* **20**(3), 3129–3143 (2012).
25. A. Greenbaum, U. Sikora, and A. Ozcan, "Field-portable wide-field microscopy of dense samples using multi-height pixel super-resolution based lensfree imaging," *Lab Chip* **12**(7), 1242–1245 (2012).
26. P. S. Sahota et al., "Approaches to improve angiogenesis in tissue-engineered skin," *Wound Repair Regen.* **12**(6), 635–642 (2004).
27. J. Folkman, "Tumor angiogenesis: therapeutic implications," *N. Engl. J. Med.* **285**(7), 1182–1186 (1971).
28. P. Carmeliet, "Angiogenesis in health and disease," *Nat. Med.* **9**(6), 653–660 (2003).
29. L. Evensen et al., "A novel imaging-based high-throughput screening approach to anti-angiogenic drug discovery," *Cytom. Part A* **77**(1), 41–51 (2010).
30. C. A. Staton, M. W. R. Reed, and N. J. Brown, "A critical analysis of current *in vitro* and *in vivo* angiogenesis assays," *Int. J. Exp. Pathol.* **90**(3), 195–221 (2009).
31. E. Kniazeva and A. J. Putnam, "Endothelial cell traction and ECM density influence both capillary morphogenesis and maintenance in 3D," *Am. J. Physiol. Cell Physiol.* **297**(1), 179–187 (2009).
32. T. Korff and H. G. Augustin, "Tensional forces in fibrillar extracellular matrices control directional capillary sprouting," *J. Cell Sci.* **112**(19), 3249–3258 (1999).
33. M. N. Nakatsu et al., "Angiogenic sprouting and capillary lumen formation modeled by human umbilical vein endothelial cells (HUVEC) in fibrin gels: the role of fibroblasts and angiopoietin-1," *Microvasc. Res.* **66**(2), 102–112 (2003).
34. V. Nehls and D. Drenckhahn, "A novel, microcarrier-based *in vitro* assay for rapid and reliable quantification of three-dimensional cell migration and angiogenesis," *Microvasc. Res.* **50**(3), 311–322 (1995).
35. A. Collen et al., "Influence of fibrin structure on the formation and maintenance of capillary-like tubules by human microvascular endothelial cells," *Angiogenesis* **2**(2), 153–165 (1998).
36. T. I. Koblizek et al., "Angiopoietin-1 induces sprouting angiogenesis *in vitro*," *Curr. Biol.* **8**(9), 529–532 (1998).
37. A. Wenger et al., "Modulation of *in vitro* angiogenesis in a three-dimensional spheroidal coculture model for bone tissue engineering," *Tissue Eng.* **10**(9–10), 1536–1547 (2004).
38. I. Arganda-Carreras et al., "3D reconstruction of histological sections: application to mammary gland tissue," *Microsc. Res. Techniq.* **73**(11), 1019–1029 (2010).
39. A. Niemisto et al., "Robust quantification of *in vitro* angiogenesis through image analysis," *IEEE Trans. Med. Imaging* **24**(4), 549–553 (2005).
40. J. Plendl et al., "Primitive endothelial cell lines from the porcine embryonic yolk sac," *In Vitro Cell Dev. Biol. Animal* **38**(6), 334–342 (2002).
41. V. Nehls and D. Drenckhahn, "A microcarrier-based cocultivation system for the investigation of factors and cells involved in angiogenesis in three-dimensional fibrin matrices *in vitro*," *Histochem. Cell Biol.* **104**(6), 459–466 (1995).
42. J. W. Goodman, *Introduction to Fourier Optics*, 3rd ed., Roberts & Company Publishers, Greenwood Village, Colo (2005).
43. L. J. Allen and M. P. Oxley, "Phase retrieval from series of images obtained by defocus variation," *Opt. Commun.* **199**(1–4), 65–75 (2001).
44. A. F. Coskun et al., "Lensfree fluorescent on-chip imaging of transgenic caenorhabditis elegans over an ultra-wide field-of-view," *PLoS One* **6**(1), e15955 (2011).